A gauge-compatible Hamiltonian splitting algorithm for particle-in-cell simulations using finite element exterior calculus

Alexander S. Glasser [1,2],† and Hong Qin[1,2]

[1]Princeton Plasma Physics Laboratory, Princeton University, Princeton, NJ 08543, USA

[2]Department of Astrophysical Sciences, Princeton University, Princeton, NJ 08544, USA

A particle-in-cell algorithm is derived with a canonical Poisson structure in the formalism of finite element exterior calculus. The resulting method belongs to the class of gauge-compatible splitting algorithms, which exactly preserve gauge symmetries and their associated conservation laws via the momentum map. We numerically demonstrate this time invariance of the momentum map and its usefulness in establishing precise initial conditions with a desired initial electric field and fixed background charge. The restriction of this canonical, finite element Poisson structure to the 1X2P $1\frac{1}{2}$-dimensional phase space is also considered and simulated numerically.

Key word: plasma simulation

---

1. Introduction

Structure-preserving particle-in-cell (PIC) algorithms preserve many of the geometric and topological mathematical structures of a point-particle kinetic plasma model, including its symplectic structure, symmetries, conservation laws and cohomology (Villasenor & Buneman 1992; Esirkepov 2001; Squire, Qin & Tang 2012; Evstatiev & Shadwick 2013; Xiao *et al.* 2013; Crouseilles, Einkemmer & Faou 2015; He *et al.* 2015; Moon, Teixeira & Omelchenko 2015; Qin *et al.* 2015, 2016; Xiao *et al.* 2015; He *et al.* 2016; Burby 2017; Kraus & Hirvijoki 2017; Kraus *et al.* 2017; Morrison 2017; Xiao, Qin & Liu 2018; Xiao & Qin 2019; Glasser & Qin 2020; Hirvijoki, Kormann & Zonta 2020; Holderied, Possanner & Wang 2021; Kormann & Sonnendrücker 2021; O'Connor *et al.* 2021; Perse, Kormann & Sonnendrücker 2021; Pinto, Kormann & Sonnendrücker 2022; Wang *et al.* 2021; Xiao & Qin 2021). One such structure, gauge symmetry, was first preserved in a PIC algorithm in the Lagrangian formalism via a variational method (Squire *et al.* 2012). More recently, it was also demonstrated that gauge symmetry could be exactly preserved in a Hamiltonian PIC algorithm via a gauge-compatible splitting method (Glasser & Qin 2020), or GCSM.

GCSMs are splitting methods whose sub-Hamiltonians H_i (satisfying $H = \sum H_i$) are each gauge symmetric and exactly numerically integrable. It can be shown that

---

† Email address for correspondence: asg5@princeton.edu

such methods preserve the momentum map (Souriau 1970; Marsden & Ratiu 1999; da Silva 2001) of a gauge-symmetric Hamiltonian system. In a GCSM PIC algorithm, the momentum map μ associated with electromagnetic gauge symmetry forms a discrete equivalent of Gauss' law, characterized by the electric field E and charge density ρ as $\mu \sim (\nabla \cdot E - 4\pi\rho)/4\pi c$ (in Gaussian units). Its preservation – $\dot{\mu} = 0$ – enforces a discrete local charge conservation law throughout the simulation domain. As we shall see, specifying this momentum map μ as an initial condition of a plasma simulation furthermore enables the precise assignment of any fixed background charge that may be desired throughout a simulation.

Most of the literature's recent structure-preserving Hamiltonian PIC methods employ a non-canonical Poisson structure to describe position and velocity particle degrees of freedom (X, V) and discrete electric and magnetic fields (E, B) (Crouseilles *et al.* 2015; He *et al.* 2015; Qin *et al.* 2015; Xiao *et al.* 2015; He *et al.* 2016; Burby 2017; Kraus & Hirvijoki 2017; Kraus *et al.* 2017; Morrison 2017; Xiao *et al.* 2018; Xiao & Qin 2019, 2021; Holderied *et al.* 2021; Kormann & Sonnendrücker 2021; Perse *et al.* 2021; Pinto *et al.* 2022). This approach hides from view the gauge symmetry of the Vlasov–Maxwell system and the simplicity of its canonical Poisson structure, characterized by the electromagnetic potential A and its conjugate momentum $Y \sim \mathrm{d}A/\mathrm{d}t$, as well as particle position and momentum, (X, P). The process of 'hiding' this gauge symmetry may be formally regarded as the Poisson reduction of the Vlasov–Maxwell system (Marsden & Weinstein 1974, 1982; Marsden & Ratiu 1986; Glasser & Qin 2020), which strips out gauge symmetry to reduce canonical coordinates (A, Y, X, P) to their non-canonical counterparts (E, B, X, V).

In this work, we demonstrate the effectiveness of the canonical formalism in simulating the Vlasov–Maxwell system. Using the flexible techniques of finite element exterior calculus (Arnold, Falk & Winther 2006, 2010) previously adopted in Kraus *et al.* (2017), we discover a canonical finite element Poisson structure for the Vlasov–Maxwell system. From this discrete structure, we derive a gauge-compatible splitting method that defines an exactly solvable symplectic PIC algorithm. We characterize the gauge symmetry of this algorithm and use it to derive the charge-conserving momentum map, μ. We further demonstrate the use of μ to establish initial conditions with a simple numerical example of a fixed, homogeneous, neutralizing, positive background charge in a Landau damping simulation. Lastly, we consider the restriction of our method to a $1\frac{1}{2}$-dimensional (Crouseilles *et al.* 2015) 1X2P phase space. We demonstrate that this subsystem retains the essential gauge structure of the Vlasov–Maxwell system, and test its numerical efficacy with a simulation of the Weibel instability (Weibel 1959).

The remainder of this article is organized as follows. In § 2, we briefly introduce the momentum map. In § 3, we describe aspects of finite element exterior calculus that are used in the algorithm. In § 4, we derive the canonical Poisson structure of the discrete Vlasov–Maxwell system, its Hamiltonian and its momentum map. In § 5, a GCSM is derived. In § 6, we describe the practical use of the momentum map, and present numerical results from Landau damping and Weibel instability simulations. In § 7, we summarize and conclude.

2. A brief review of the momentum map

The momentum map (Souriau 1970; Marsden & Ratiu 1999; da Silva 2001) may be viewed as the Hamiltonian manifestation of the Noether principle – i.e. that every smooth symmetry of a dynamical system corresponds to a conserved quantity. We may demonstrate how the momentum map arises from the symmetry transformations of a Lie group on a Poisson manifold, as follows.

Suppose a Poisson manifold M is equipped with symmetry transformations defined by the group action $\Phi : G \times M \to M$, where G is a Lie group whose elements act upon M. The group action Φ_g associated with any fixed $g \in G$ is defined such that $\Phi_g(x) = \Phi(g, x) \; \forall \; x \in M$. The corresponding Lie algebra $\mathfrak{g} = \mathrm{Lie}(G)$, may be regarded as generating these symmetry transformations, since $\forall \; s \in \mathfrak{g}$ there exists a vector field $X_s \in \mathfrak{X}(M)$ on M defined by

$$X_s = \left. \frac{\mathrm{d}}{\mathrm{d}\epsilon} \right|_{\epsilon=0} \Phi_{\exp(\epsilon s)}. \tag{2.1}$$

Here, $\{\exp(\epsilon s) \in G \mid \epsilon \in \mathbb{R}\}$ is the one-parameter subgroup of G generated by s. Thus, the vector field X_s is seen to 'infinitesimally generate' the family of symmetry transformations $\Phi_{\exp(\epsilon s)}$. Equivalently, one may regard the collection of maps $\{\Phi_{\exp(\epsilon s)} : M \to M \mid \epsilon \in \mathbb{R}\}$ as the flow of M along the vector field X_s. In this way, each Lie algebra generator $s \in \mathfrak{g}$ corresponds to a generator of transformations on M – namely, the vector field X_s.

Now suppose $\{\cdot, \cdot\} : C^\infty(M) \times C^\infty(M) \to C^\infty(M)$ denotes the Poisson bracket on M, defining an algebra of smooth functions. The momentum map is then defined as a linear map $\mu : \mathfrak{g} \to C^\infty(M)$ which assigns to every $s \in \mathfrak{g}$ a generating function $\mu(s) \in C^\infty(M)$ – henceforth denoted $\mu_s = \mu(s)$ – satisfying

$$\{F, \mu_s\} = X_s(F) \quad \forall \; F \in C^\infty(M). \tag{2.2}$$

Here, $X_s(F)$ denotes the Lie derivative of F by the vector field X_s. In this way, μ_s is a generating function via the Poisson bracket for the symmetry transformation generated by s; in particular, $X_s = \{\cdot, \mu_s\}$ are equal as derivations on $C^\infty(M)$. Therefore, when a momentum map μ is defined, each $s \in \mathfrak{g}$ corresponds not only to a vector field X_s on M, but to a generating function $\mu_s \in C^\infty(M)$ as well. The linearity of μ implies that $\mu_{s+t} = \mu_s + \mu_t$, and we more generally denote μ as the map satisfying $\mu \cdot s = \mu_s \; \forall \; s \in \mathfrak{g}$.

In a symmetric Hamiltonian system, the function μ_s is not only a generator of a symmetry transformation, but also a conserved quantity. To see this, consider a symmetric Hamiltonian $H \in C^\infty(M)$ that is invariant under a group action Φ, such that

$$H \circ \Phi_g = H \quad \forall \; g \in G. \tag{2.3}$$

Setting $g = \exp(\epsilon s)$ and differentiating both sides of (2.3) with respect to ϵ, it follows by (2.1) that $X_s(H) = 0 \; \forall \; s \in \mathfrak{g}$. By (2.2), then,

$$0 = \{H, \mu_s\} = -\dot{\mu}_s. \tag{2.4}$$

Therefore, μ_s is constant along the flow generated by H on M, i.e. it is conserved in time. Since $0 = \dot{\mu}^s = \mathrm{d}/\mathrm{d}t(\mu \cdot s) = \dot{\mu} \cdot s \; \forall \; s \in \mathfrak{g}$, we more generally write that $\dot{\mu} = 0$.

3. Relevant aspects of finite element exterior calculus

We now introduce notation and briefly describe elementary aspects of finite element exterior calculus (Arnold *et al.* 2006, 2010), abbreviated FEEC. To approximate differential forms on a smooth manifold Ω by finite elements, FEEC projects the de Rham complex of differential forms $0 \xrightarrow{\mathrm{d}} \Lambda^0(\Omega) \xrightarrow{\mathrm{d}} \cdots \xrightarrow{\mathrm{d}} \Lambda^n(\Omega) \xrightarrow{\mathrm{d}} 0$ onto spaces of piecewise polynomial differential forms, as depicted in figure 1. In particular, given a triangulation of Ω denoted $\mathcal{T}_h$ (with maximum diameter h on any given cell), $\Lambda^p(\mathcal{T}_h)$ denotes some finite-dimensional space of piecewise p-forms on $\mathcal{T}_h$ whose coefficients are polynomial over each p-cell of $\mathcal{T}_h$. The projection map $\pi_h : \Lambda^p(\Omega) \to \Lambda^p(\mathcal{T}_h)$ for each p is required to ensure that the diagram of figure 1 commutes – in particular, that

$$0 \xrightarrow{\mathrm{d}} \Lambda^0(\Omega) \xrightarrow{\mathrm{d}} \cdots \xrightarrow{\mathrm{d}} \Lambda^n(\Omega) \xrightarrow{\mathrm{d}} 0$$

$$\pi_h \downarrow \qquad\qquad\qquad \pi_h \downarrow$$

$$0 \xrightarrow{\mathrm{d}} \Lambda^0(\mathcal{T}_h) \xrightarrow{\mathrm{d}} \cdots \xrightarrow{\mathrm{d}} \Lambda^n(\mathcal{T}_h) \xrightarrow{\mathrm{d}} 0$$
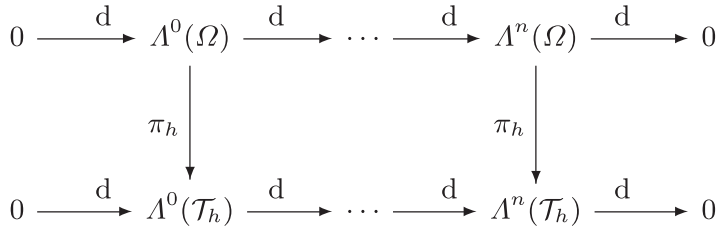
FIGURE 1. Given a triangulation $\mathcal{T}_h$ of the smooth manifold Ω, each space of differential forms $\Lambda^p(\Omega)$ of the continuous cochain complex is projected onto a finite element space $\Lambda^p(\mathcal{T}_h)$. There are many possible choices, of varying degrees of accuracy, for the spaces of piecewise polynomial finite elements $\Lambda^p(\mathcal{T}_h)$. The projections π_h are required to satisfy $\pi_h \circ \mathrm{d} = \mathrm{d} \circ \pi_h$, such that the diagram above is commuting.

$\pi_h \circ \mathrm{d} = \mathrm{d} \circ \pi_h$. The horizontal arrows of figure 1 are required to form cochain complexes ($\mathrm{d} \circ \mathrm{d} = 0$) such that the projections π_h are isomorphisms of cohomology. There exist many possible choices for the finite element spaces $\Lambda^p(\mathcal{T}_h)$, which can vary in their degree of accuracy and with the choice of triangulation $\mathcal{T}_h$. However, any such choice must ensure that the sequence of spaces $\cdots \to \Lambda^p(\mathcal{T}_h) \to \cdots$ constitutes a cochain complex, and that the finite element problem being studied is solvable and well posed in those spaces.

For example, a straightforward choice for $\Lambda^p(\mathcal{T}_h)$ is given by the space of all piecewise polynomial p-forms of degree $\leqslant r$, denoted $\mathcal{P}_r \Lambda^p(\mathcal{T}_h)$. An alternative, more lightweight choice for $\Lambda^p(\mathcal{T}_h)$ is the space of Whitney p-forms (Whitney 1957). These are piecewise linear forms that can be defined using barycentric coordinate functions $\{\lambda_0, \ldots, \lambda_p\}$ such that, for any p-simplex σ, the Whitney p-form ϕ_σ associated with σ is given by

$$\phi_\sigma = \sum_{i=0}^{p} (-1)^i \lambda_{\sigma(i)} [\mathrm{d}\lambda_{\sigma(0)} \wedge \cdots \wedge \widehat{\mathrm{d}\lambda_{\sigma(i)}} \wedge \cdots \wedge \mathrm{d}\lambda_{\sigma(p)}]. \tag{3.1}$$

(Here, the hat signifies that $\mathrm{d}\lambda_{\sigma(i)}$ is omitted.) We refer the reader to Arnold *et al.* (2006, 2010), Arnold & Awanou (2013) and Arnold, Boffi & Bonizzoni (2015) for more detailed descriptions of cochain-complex-conforming finite element spaces.

We may fix a notation for calculations with finite elements independent of the choice of space $\Lambda^p(\mathcal{T}_h)$. For any such choice, we may fix a basis for $\Lambda^p(\mathcal{T}_h)$ with N_p finite elements, and organize them into the $N_p \times 1$ vector $\boldsymbol{\Lambda}^p$. The ith entry of $\boldsymbol{\Lambda}^p$ is a basis element we denote $\Lambda_i^p \in \Lambda^p(\mathcal{T}_h)$, which defines a piecewise polynomial p-form on $\mathcal{T}_h$. Any p-form $\boldsymbol{S} \in \Lambda^p(\mathcal{T}_h)$ may thus be expanded in the $\boldsymbol{\Lambda}^p$ basis as

$$\boldsymbol{S}(\boldsymbol{x}) = \boldsymbol{s} \cdot \boldsymbol{\Lambda}^p(\boldsymbol{x}) = s_i \Lambda_i^p(\boldsymbol{x}) \tag{3.2}$$

$\forall \boldsymbol{x} \in |\mathcal{T}_h|$ (where $|\mathcal{T}_h| \subset \mathbb{R}^n$ denotes the convex hull of $\mathcal{T}_h$). The individual components of $\boldsymbol{S}$ will be denoted

$$\boldsymbol{S}(\boldsymbol{x})_{\mu_1 \cdots \mu_p} = \boldsymbol{s} \cdot \boldsymbol{\Lambda}^p(\boldsymbol{x})_{\mu_1 \cdots \mu_p} = s_i \Lambda_i^p(\boldsymbol{x})_{\mu_1 \cdots \mu_p}. \tag{3.3}$$

Here, $\boldsymbol{s} \in \mathbb{R}^{N_p}$ and Einstein summation convention is used for the repeated i index. Greek letters denote coordinate indices. For $|\mathcal{T}_h| \subset \mathbb{R}^3$, for example, the μth component of the 1-form basis element $\Lambda_i^1(\boldsymbol{x})$ is denoted $\Lambda_i^1(\boldsymbol{x})_\mu$ $\forall$ $\mu \in \{1, 2, 3\}$, such that $\Lambda_i^1(\boldsymbol{x}) = \Lambda_i^1(\boldsymbol{x})_\mu \, \mathrm{d}x^\mu$.

Exterior calculus may be computed in the $\boldsymbol{\Lambda}^0, \ldots, \boldsymbol{\Lambda}^n$ bases by simple matrix multiplication. Let us define this explicitly on $\mathbb{R}^3$, where the exterior derivatives of 0-, 1-

p-Form	Abstract d	Matrix d	Definition	Dimensions
$\boldsymbol{S} = \boldsymbol{s} \cdot \boldsymbol{\Lambda}^0$	—	—	—	—
$\boldsymbol{A} = \boldsymbol{a} \cdot \boldsymbol{\Lambda}^1$	$\boldsymbol{A} = \mathrm{d}\boldsymbol{S}$	$\boldsymbol{a} = \mathbb{G}\boldsymbol{s}$	$\mathbb{G}^T \boldsymbol{\Lambda}^1 = \mathrm{d}\boldsymbol{\Lambda}^0$	$\mathbb{G} \in \mathbb{R}^{N_1 \times N_0}$
$\boldsymbol{B} = \boldsymbol{b} \cdot \boldsymbol{\Lambda}^2$	$\boldsymbol{B} = \mathrm{d}\boldsymbol{A}$	$\boldsymbol{b} = \mathbb{C}\boldsymbol{a}$	$\mathbb{C}^T \boldsymbol{\Lambda}^2 = \mathrm{d}\boldsymbol{\Lambda}^1$	$\mathbb{C} \in \mathbb{R}^{N_2 \times N_1}$
$\boldsymbol{C} = \boldsymbol{c} \cdot \boldsymbol{\Lambda}^3$	$\boldsymbol{C} = \mathrm{d}\boldsymbol{B}$	$\boldsymbol{c} = \mathbb{D}\boldsymbol{b}$	$\mathbb{D}^T \boldsymbol{\Lambda}^3 = \mathrm{d}\boldsymbol{\Lambda}^2$	$\mathbb{D} \in \mathbb{R}^{N_3 \times N_2}$

TABLE 1. The finite element matrix implementation of d on $\mathbb{R}^3$. The property $\mathrm{d} \circ \mathrm{d} = 0$ implies that $\mathbb{C}\mathbb{G} = 0$ and $\mathbb{D}\mathbb{C} = 0$.

and 2-forms can be implemented via matrices that represent the gradient ($\mathbb{G}$), curl ($\mathbb{C}$) and divergence ($\mathbb{D}$), respectively. In table 1, we define these matrices to act on the coefficients of forms so as to compute the forms' exterior derivatives. For example, the gradient of the 0-form $\boldsymbol{S} = \boldsymbol{s} \cdot \boldsymbol{\Lambda}^0$ is computed to be $\mathrm{d}\boldsymbol{S} = \mathbb{G}\boldsymbol{s} \cdot \boldsymbol{\Lambda}^1$, where the matrix $\mathbb{G} \in \mathbb{R}^{N_1 \times N_0}$ is defined such that $\mathrm{d}\boldsymbol{\Lambda}^0 = \mathbb{G}^T \boldsymbol{\Lambda}^1$. This definition gives the desired result since

$$\mathrm{d}\boldsymbol{S} = \boldsymbol{s} \cdot \mathrm{d}\boldsymbol{\Lambda}^0 = \boldsymbol{s} \cdot \mathbb{G}^T \boldsymbol{\Lambda}^1 = \mathbb{G}\boldsymbol{s} \cdot \boldsymbol{\Lambda}^1. \tag{3.4}$$

Lastly, it will be useful to define the mass matrix on $\mathcal{T}_h$ for each basis $\boldsymbol{\Lambda}^p$ of finite element p-forms. Specifically, we define the mass matrix $\mathbb{M}_p \in \mathbb{R}^{N_p \times N_p}$ of $\boldsymbol{\Lambda}^p$ by

$$(\mathbb{M}_p)_{ij} = \int_{|\mathcal{T}_h|} \mathrm{d}\boldsymbol{x} \left(\Lambda_i^p, \Lambda_j^p \right)_p = \int_{|\mathcal{T}_h|} \Lambda_i^p \wedge \star \Lambda_j^p. \tag{3.5}$$

Here, $(\cdot, \cdot)_p$ denotes the inner product on p-forms induced by the metric $g_{\mu\nu}$, namely

$$\begin{aligned}
(\alpha, \beta)_p &= \frac{1}{p!} \alpha_{\mu_1 \cdots \mu_p} \beta^{\mu_1 \cdots \mu_p} \\
&= \frac{1}{p!} \alpha_{\mu_1 \cdots \mu_p} \beta_{\nu_1 \cdots \nu_p} g^{\mu_1 \nu_1} \cdots g^{\mu_p \nu_p}.
\end{aligned} \tag{3.6}$$

On $\mathbb{R}^3$, for example, (3.6) defines $(\alpha, \beta)_p$ for $p = 1, 2$ simply as the standard inner product $\alpha \cdot \beta$. After all, 1- and 2-forms each have three independent components on $\mathbb{R}^3$ and $g_{\mu\nu} = \delta_{\mu\nu}$. We note that $(\alpha, \beta)_p$ is symmetric, such that $\mathbb{M}_p^T = \mathbb{M}_p$. Equation (3.5) may be understood to define the Hodge star operator $\star$, such that $\alpha \wedge \star \beta = (\alpha, \beta)_p \, \mathrm{d}\boldsymbol{x}$ for arbitrary p-forms α and β, where $\mathrm{d}\boldsymbol{x}$ denotes the unique volume form that evaluates to unity on positively oriented vectors that are orthonormal with respect to $g_{\mu\nu}$. The mass matrix will evidently appear wherever metric information is incorporated via the Hodge star.

4. A discrete Vlasov–Maxwell Poisson structure and Hamiltonian

We now apply the formalism above to define a canonical finite element Poisson structure and Hamiltonian for the Vlasov–Maxwell system. We first describe the Poisson structure of discrete electromagnetic fields on a triangulation $\mathcal{T}_h$ of the spatial manifold $\Omega \subset \mathbb{R}^3$.

4.1. *The finite element electromagnetic Poisson structure*

To start, let us consider electromagnetic fields on the continuous manifold Ω, using the temporal gauge wherein the electric potential vanishes, $\phi = 0$. The configuration space for such fields is the set $Q = \{A \mid A \in \Lambda^1(\Omega)\}$ of possible vector potentials, defined

as differential 1-forms over Ω. To find a variable conjugate to $A(x)$, we compute the following variational derivative of the electromagnetic Lagrangian expressed in Gaussian units,

$$L_{\text{EM}} = \frac{1}{8\pi} \int \mathrm{d}x \left(\left| -\frac{1}{c}\dot{A} \right|^2 - |\mathrm{d}A|^2 \right), \quad Y = \frac{\delta L_{\text{EM}}}{\delta \dot{A}} = \frac{\dot{A}}{4\pi c^2}. \tag{4.1a,b}$$

Clearly, $Y \in \Lambda^1(\Omega)$ is also a 1-form over Ω corresponding to negative the electric field, $Y = -E/4\pi c$. As in (3.6), $|\alpha|^2 = (\alpha, \alpha)_p$ in (4.1a) denotes the standard inner product on $\mathbb{R}^3$ for $p = 1, 2$.

The full phase space is then given by the cotangent bundle $T^*Q = \{A, Y\}$ whose canonical symplectic structure is defined by the Poisson bracket (Marsden & Weinstein 1982)

$$\{F, G\} = \int \left(\frac{\delta F}{\delta A} \cdot \frac{\delta G}{\delta Y} - \frac{\delta G}{\delta A} \cdot \frac{\delta F}{\delta Y} \right) \mathrm{d}x. \tag{4.2}$$

Here, $F[A, Y]$ and $G[A, Y]$ are arbitrary functionals on T^*Q.

We now map this geometric description of fields on Ω to its triangulation $\mathcal{T}_h$. On $\mathcal{T}_h$, the fields A and Y can be defined by their expansion in the corresponding basis for finite element 1-forms

$$\left.\begin{array}{l} A(t, x) = a(t) \cdot \Lambda^1(x) \\[2mm] Y(t, x) = y(t) \cdot \mathbb{M}_1^{-1} \cdot \Lambda^1(x). \end{array}\right\} \tag{4.3}$$

Here, Λ^1 is an $N_1 \times 1$ vector of basis elements and $a, y \in \mathbb{R}^{N_1}$ denote coefficients, as in (3.2). a and y are identified as dynamical variables by explicitly notating their time dependence. The inverse factor of the 1-form mass matrix $\mathbb{M}_1$ in (4.3) follows from computing the conjugate momentum of a in the following discretization of L_{EM}:

$$\begin{aligned} L_{\text{EM}} &= \frac{1}{8\pi} \int_{|\mathcal{T}_h|} \mathrm{d}x \left(\left| -\frac{1}{c}\dot{a} \cdot \Lambda^1 \right|^2 - |a \cdot \mathrm{d}\Lambda^1|^2 \right) \\ &= \frac{1}{8\pi} \int_{|\mathcal{T}_h|} \mathrm{d}x \left(\frac{1}{c^2}\dot{a} \cdot \mathbb{M}_1 \cdot \dot{a} - a \cdot \mathbb{C}^T \mathbb{M}_2 \mathbb{C} \cdot a \right), \quad y = \frac{\delta L_{\text{EM}}}{\delta \dot{a}} = \frac{\mathbb{M}_1 \dot{a}}{4\pi c^2}, \quad (4.4a,b) \end{aligned}$$

where we have substituted $\mathrm{d}\Lambda^1 = \mathbb{C}^T \Lambda^2$ from table 1 and used mass matrices as defined in (3.5). Comparing (4.1a,b) and (4.4) yields the desired expansion for Y in (4.3). (This inverse factor of $\mathbb{M}_1$ will further ensure that the Poisson bracket of (4.9) is canonical.)

To discretize the Poisson bracket of (4.2), we must first express $\delta F/\delta A$ in terms of $\partial F/\partial a$ for a discrete variation $\delta A = \delta a \cdot \Lambda^1$. Since variational derivatives are valued dually to their variations, following Kraus *et al.* (2017), it is appropriate to require that

$$\left\langle \frac{\delta F}{\delta A}, \delta a \cdot \Lambda^1 \right\rangle_{L^2 \Lambda^1} = \left\langle \frac{\partial F}{\partial a}, \delta a \right\rangle_{\mathbb{R}^{N_1}}. \tag{4.5}$$

Here, $\langle \cdot, \cdot \rangle_{L^2 \Lambda^1} = \int_{|\mathcal{T}_h|} \mathrm{d}x (\cdot, \cdot)_{p=1}$ denotes the $L^2 \Lambda^1$ inner product, and $\langle \cdot, \cdot \rangle_{\mathbb{R}^{N_1}}$ the standard inner product on $\mathbb{R}^{N_1}$. In particular, setting $\delta a_j = \delta_{ij}$ for some fixed, arbitrary $i \in [1, N_1]$

and using $(\cdot, \cdot)_p$ as defined in (3.6), (4.5) yields

$$\int_{|\mathcal{T}_h|} d\boldsymbol{x} \left(\frac{\delta F}{\delta \boldsymbol{A}}, \Lambda_i^1(\boldsymbol{x}) \right)_{p=1} = \frac{\partial F}{\partial a_i}. \tag{4.6}$$

To solve for $\delta F / \delta \boldsymbol{A}$, we expand $\delta F / \delta \boldsymbol{A} = \boldsymbol{f} \cdot \boldsymbol{\Lambda}^1$ in the $\boldsymbol{\Lambda}^1$ basis for some $\boldsymbol{f} \in \mathbb{R}^{N_1}$, such that evaluating (4.6) implies $\boldsymbol{f} = \mathbb{M}_1^{-1} \cdot \partial F / \partial \boldsymbol{a}$. Therefore,

$$\frac{\delta F}{\delta \boldsymbol{A}} = \frac{\partial F}{\partial \boldsymbol{a}} \cdot \mathbb{M}_1^{-1} \cdot \boldsymbol{\Lambda}^1. \tag{4.7}$$

The discrete variation $\delta \boldsymbol{Y} = \delta \boldsymbol{y} \cdot \mathbb{M}_1^{-1} \cdot \boldsymbol{\Lambda}^1$ establishes a similar result for $\boldsymbol{Y}$, namely

$$\frac{\delta F}{\delta \boldsymbol{Y}} = \frac{\partial F}{\partial \boldsymbol{y}} \cdot \boldsymbol{\Lambda}^1. \tag{4.8}$$

Thus, to derive the discrete Poisson bracket, we substitute (4.7)–(4.8) into (4.2) and integrate over $|\mathcal{T}_h|$ to find

$$\{F, G\} = \frac{\partial F}{\partial \boldsymbol{a}} \cdot \frac{\partial G}{\partial \boldsymbol{y}} - \frac{\partial G}{\partial \boldsymbol{a}} \cdot \frac{\partial F}{\partial \boldsymbol{y}}. \tag{4.9}$$

True to its continuous counterpart in (4.2), the discrete Poisson bracket of (4.9) is in canonical symplectic form (i.e. Darboux coordinates).

4.2. *The finite element Vlasov–Maxwell system*

The full Poisson structure of the discrete Vlasov–Maxwell system readily follows from the foregoing analysis of its electromagnetic subsystem. To describe a system of L particles, we let $\boldsymbol{X}_\ell, \boldsymbol{P}_\ell \in \mathbb{R}^3$ $\ell \in [1, L]$ denote the position and momentum of the ℓth particle and let m_ℓ and q_ℓ denote its mass and charge. Particles may then be characterized by a Klimontovich distribution, $f(\boldsymbol{x}, \boldsymbol{p}) = \sum_\ell \delta(\boldsymbol{x} - \boldsymbol{X}_\ell) \delta(\boldsymbol{p} - \boldsymbol{P}_\ell)$. Particle phase space is defined as usual with a canonical bracket on position $\boldsymbol{X}_\ell$ and momentum $\boldsymbol{P}_\ell$.

Combining (4.9) with the Poisson bracket for these L particles, therefore, the discrete Vlasov–Maxwell Poisson structure is given by

$$\{F, G\} = \frac{\partial F}{\partial \boldsymbol{a}} \cdot \frac{\partial G}{\partial \boldsymbol{y}} - \frac{\partial G}{\partial \boldsymbol{a}} \cdot \frac{\partial F}{\partial \boldsymbol{y}} + \sum_{\ell=1}^{L} \left(\frac{\partial F}{\partial \boldsymbol{X}_\ell} \cdot \frac{\partial G}{\partial \boldsymbol{P}_\ell} - \frac{\partial G}{\partial \boldsymbol{X}_\ell} \cdot \frac{\partial F}{\partial \boldsymbol{P}_\ell} \right). \tag{4.10}$$

Here, F and G are arbitrary functionals on the discrete Poisson manifold $(M_d, \{\cdot, \cdot\})$, where each point $m_d \in M_d$ is defined by the data

$$m_d = (\boldsymbol{a}, \boldsymbol{y}, \boldsymbol{X}_1, \dots, \boldsymbol{X}_L, \boldsymbol{P}_1, \dots, \boldsymbol{P}_L)$$
$$\in \mathbb{R}^{N_1} \times \mathbb{R}^{N_1} \times \mathbb{R}^{3L} \times \mathbb{R}^{3L}. \tag{4.11}$$

We now define a Hamiltonian $H_{\text{VM}} = H_{\text{VM}}[\boldsymbol{a}, \boldsymbol{y}, \boldsymbol{X}_i, \boldsymbol{P}_i]$ on M_d, given in Gaussian units by

$$
\left.
\begin{aligned}
H_{\text{VM}} &= H_{\text{EM}} + H_{\text{Kinetic}} \\
\text{where} \quad H_{\text{EM}} &= \frac{1}{8\pi} \int_{|\mathcal{T}_h|} \mathrm{d}\boldsymbol{x} \left(|-4\pi c \boldsymbol{Y}|^2 + |\mathrm{d}\boldsymbol{A}|^2 \right) \\
&= \frac{1}{8\pi} \left((4\pi c)^2 \boldsymbol{y} \cdot \mathbb{M}_1^{-1} \cdot \boldsymbol{y} + \boldsymbol{a} \cdot \mathbb{C}^T \mathbb{M}_2 \mathbb{C} \cdot \boldsymbol{a} \right) \\
H_{\text{Kinetic}} &= \sum_{\ell=1}^{L} \frac{1}{2m_\ell} \left| \boldsymbol{P}_\ell - \frac{q_\ell}{c} A(\boldsymbol{X}_\ell) \right|^2
\end{aligned}
\right\}, \tag{4.12}
$$

where $A(\boldsymbol{X}_\ell) = \boldsymbol{a} \cdot \boldsymbol{\Lambda}^1(\boldsymbol{X}_\ell)$. In H_{EM}, we have substituted (3.5) and (4.3). The difference in H_{Kinetic} is taken componentwise, i.e. $P_{\ell\mu} - (q_\ell/c)\boldsymbol{a} \cdot \boldsymbol{\Lambda}^1(\boldsymbol{X}_\ell)_\mu$ for $\mu \in \{1, 2, 3\}$. Hereafter, we denote components of $\boldsymbol{P}_\ell$ by $P_{\ell\mu}$ and those of $\boldsymbol{X}_\ell$ by X_ℓ^μ.

4.3. *Gauge structure*

We now examine the gauge structure of this discrete Vlasov–Maxwell system and derive its corresponding momentum map. We first note that, because $\mathbb{C}\mathbb{G} = 0$, H_{VM} of (4.12) is invariant under any gauge transformation $\Phi_{\exp(s)} : M_d \to M_d$ of the form

$$
\Phi_{\exp(s)} \begin{pmatrix} \boldsymbol{a} \\ \boldsymbol{y} \\ \boldsymbol{X}_\ell \\ \boldsymbol{P}_\ell \end{pmatrix} = \begin{pmatrix} \boldsymbol{a} + \mathbb{G}\boldsymbol{s} \\ \boldsymbol{y} \\ \boldsymbol{X}_\ell \\ \boldsymbol{P}_\ell + \frac{q_\ell}{c}\mathbb{G}\boldsymbol{s} \cdot \boldsymbol{\Lambda}^1(\boldsymbol{X}_\ell) \end{pmatrix} \tag{4.13}
$$

$\forall \ \ell \in [1, L]$, $\boldsymbol{s} \in \mathbb{R}^{N_0}$. Since $\Phi_{\exp(s)} \circ \Phi_{\exp(t)} = \Phi_{\exp(s+t)}$, such transformations form an abelian group. Evidently, they are also generated by vector fields $X_s \in \mathfrak{X}(M_d)$ of the form

$$
X_s = \frac{\mathrm{d}}{\mathrm{d}\epsilon}\Big|_{\epsilon=0} \Phi_{\exp(\epsilon s)} = \mathbb{G}_{jk}s_k \left[\partial_{a_j} + \sum_{\ell=1}^{L} \frac{q_\ell}{c} \Lambda_j^1(\boldsymbol{X}_\ell)_\mu \partial_{P_{\ell\mu}} \right], \tag{4.14}
$$

expressed using Einstein summation convention.

We may check whether Φ of (4.13) is a canonical transformation, that is, whether it preserves the Poisson bracket of (4.10)

$$
\{F, G\} \circ \Phi_{\exp(s)} = \{F \circ \Phi_{\exp(s)}, G \circ \Phi_{\exp(s)}\} \tag{4.15}
$$

$\forall \ \boldsymbol{s}$. It suffices to check this condition infinitesimally, i.e. whether

$$
X_s(\{F, G\}) = \{X_s(F), G\} + \{F, X_s(G)\}. \tag{4.16}
$$

After cancelling terms by the equality of mixed partials, verifying (4.16) reduces to checking that

$$
0 = \sum_{\ell=1}^{L} \frac{q_\ell}{c} \mathbb{G}_{jk}s_k \left[\partial_{X_\ell^\nu} \Lambda_j^1(\boldsymbol{X}_\ell)_\mu - \partial_{X_\ell^\mu} \Lambda_j^1(\boldsymbol{X}_\ell)_\nu \right] (\partial_{P_{\ell\mu}} F)(\partial_{P_{\ell\nu}} G)
$$

$$
= \sum_{\ell=1}^{L} \frac{q_\ell}{c} \left[\mathbb{G}\boldsymbol{s} \cdot \mathrm{d}\boldsymbol{\Lambda}^1(\boldsymbol{X}_\ell)_{\nu\mu} \right] (\partial_{P_{\ell\mu}} F)(\partial_{P_{\ell\nu}} G). \tag{4.17}
$$

Each term in this sum is seen to vanish, however, since

$$\mathbb{G}\boldsymbol{s} \cdot \mathrm{d}\boldsymbol{\Lambda}^1 = \boldsymbol{s} \cdot \mathbb{G}^T \mathrm{d}\boldsymbol{\Lambda}^1 = \boldsymbol{s} \cdot \mathrm{d}(\mathbb{G}^T \boldsymbol{\Lambda}^1) = \boldsymbol{s} \cdot \mathrm{dd}\boldsymbol{\Lambda}^0 = 0. \tag{4.18}$$

Thus, X_s generates a canonical group action, as desired.

We now find the momentum map μ of this canonical group action by solving for its generating functions. In particular, given any $\boldsymbol{s} \in \mathbb{R}^{N_0}$, we seek a generating function μ_s such that $X_s = \{\cdot, \mu_s\}$ as derivations, as in (2.2). By comparing (4.10) and (4.14), we see that $X_s = \{\cdot, \mu_s\}$ holds if and only if

$$\left. \begin{aligned} \frac{\partial \mu_s}{\partial \boldsymbol{a}} &= 0 \\ \frac{\partial \mu_s}{\partial \boldsymbol{y}} &= \mathbb{G}\boldsymbol{s} \\ \frac{\partial \mu_s}{\partial \boldsymbol{X}_\ell} &= -\frac{q_\ell}{c}\mathbb{G}\boldsymbol{s} \cdot \boldsymbol{\Lambda}^1(X_\ell) \\ \frac{\partial \mu_s}{\partial \boldsymbol{P}_\ell} &= 0 \quad \forall \ell \in [1, L]. \end{aligned} \right\} \tag{4.19}$$

Since $\mathbb{G}^T \boldsymbol{\Lambda}^1 = \mathrm{d}\boldsymbol{\Lambda}^0$ is an exact form, this linear system of partial differential equations is readily solved by

$$\mu_s = \mathbb{G}\boldsymbol{s} \cdot \boldsymbol{y} - \sum_{\ell=1}^{L} \frac{q_\ell}{c}\boldsymbol{s} \cdot \boldsymbol{\Lambda}^0(X_\ell). \tag{4.20}$$

The momentum map μ characterizing all generating functions $\{\mu_s\}$ is defined by requiring that $\mu \cdot \boldsymbol{s} = \mu_s \; \forall \boldsymbol{s}$. Therefore, μ is given by

$$\mu = \mathbb{G}^T \boldsymbol{y} - \sum_{\ell=1}^{L} \frac{q_\ell}{c}\boldsymbol{\Lambda}^0(X_\ell). \tag{4.21}$$

Setting $\mu = 0$, (4.21) is a discrete form of Gauss' law,

$$0 = (\boldsymbol{\nabla} \cdot \boldsymbol{E} - 4\pi\rho)/4\pi c, \tag{4.22}$$

where $\boldsymbol{E} = -4\pi c \boldsymbol{Y}$ and $\rho = \sum_\ell q_\ell \boldsymbol{\Lambda}^0(X_\ell)$.

Any non-zero value of μ indicates that the divergence of the electric field is not entirely accounted for by the dynamical particles labelled $\ell \in [1, L]$. Since $\dot{\mu} = 0$, such a non-zero μ acts as a fixed, external, non-dynamical background charge that persists throughout a simulation, and in a manner that remains entirely structure preserving. In particular, we may regard μ as representing an external charge density,

$$\mu \sim \rho_{\text{ext}}/c. \tag{4.23}$$

As we shall demonstrate, (4.23) can be useful in establishing precise initial conditions in a PIC simulation.

5. Equations of motion

5.1. *Continuous-time equations of motion*

Let us now derive equations of motion via the Hamiltonian of (4.12) and the Poisson bracket of (4.10). We find

$$
\left.
\begin{aligned}
\dot{X}_\ell^\mu &= \{X_\ell^\mu, H_{\mathrm{VM}}\} = \frac{1}{m_\ell}\left(P_{\ell\mu} - \frac{q_\ell}{c}A(X_\ell)_\mu\right) \\
\dot{P}_{\ell\mu} &= \{P_{\ell\mu}, H_{\mathrm{VM}}\} = \frac{q_\ell}{c}\dot{X}_\ell^\nu \partial_{X_\ell^\mu}A(X_\ell)_\nu \\
\dot{a} &= \{a, H_{\mathrm{VM}}\} = 4\pi c^2 \mathbb{M}_1^{-1}\cdot y \\
\dot{y} &= \{y, H_{\mathrm{VM}}\} = -\frac{1}{4\pi}\mathbb{C}^T\mathbb{M}_2\mathbb{C}\cdot a + \sum_{\ell=1}^{L}\frac{q_\ell}{c}\dot{X}_\ell^\mu \boldsymbol{\Lambda}^1(X_\ell)_\mu
\end{aligned}
\right\},
\tag{5.1}
$$

where $A(X_\ell)_\mu = a\cdot\boldsymbol{\Lambda}^1(X_\ell)_\mu$ using the component notation of (3.3).

We remark that these equations of motion allow us to reexpress the conservation of the momentum map, $\dot{\mu} = 0$, as a discrete, local charge conservation law in conservative form. In particular, we may take the time derivative $\dot{\mu}$ of (4.21) and substitute $\dot{y}$ of (5.1), noting that $\mathbb{C}\mathbb{G} = 0$ to find

$$
(\mathbb{G}^T j - \dot{\rho})/c = 0,
\tag{5.2}
$$

where $\rho = \sum_\ell q_\ell\boldsymbol{\Lambda}^0(X_\ell)$ and $j = \sum_\ell q_\ell\dot{X}_\ell^\mu\boldsymbol{\Lambda}^1(X_\ell)_\mu$. As in (4.21), we note a correspondence between the discrete and continuous operators $\mathbb{G}^T \sim (-\nabla\cdot)$. Thus, (5.2) is a discrete equivalent of the charge conservation law $\partial_t\rho + \nabla\cdot j = 0$, as seen in Kraus *et al.* (2017).

Equation (5.1) is sometimes referred to as a semi-discrete system, since it describes a discretely defined system evolving in continuous time. We now proceed to a fully discrete, algorithmic system by defining a GCSM.

5.2. *Discrete-time equations of motion via a gauge-compatible splitting*

Using the Vlasov–Maxwell splitting discovered in He *et al.* (2015) and adapted to canonical coordinates in Glasser & Qin (2020), we split H_{VM} of (4.12) into five sub-Hamiltonians, as follows:

$$
\left.
\begin{aligned}
H_{\mathrm{VM}} &= H_A + H_Y + H_{\mathrm{Kinetic}}^x + H_{\mathrm{Kinetic}}^y + H_{\mathrm{Kinetic}}^z \\
\text{where}\quad H_A &= \frac{1}{8\pi}a\cdot\mathbb{C}^T\mathbb{M}_2\mathbb{C}\cdot a \\
H_Y &= \frac{1}{8\pi}(4\pi c)^2 y\cdot\mathbb{M}_1^{-1}\cdot y \\
H_{\mathrm{Kinetic}}^\alpha &= \sum_{\ell=1}^{L}\frac{1}{2m_\ell}\left(P_{\ell\alpha} - \frac{q_\ell}{c}A(X_\ell)_\alpha\right)^2
\end{aligned}
\right\}
\tag{5.3}
$$

$\forall\ \alpha \in \{x, y, z\}$. We immediately observe that each sub-Hamiltonian remains invariant under the gauge transformation $\Phi_{\exp(s)}$ defined in (4.13).

Let us now examine the equations of motion of each subsystem, omitting equations for the subsystems' static degrees of freedom

$$
\left.
\begin{aligned}
H_A : \ & \dot{\boldsymbol{y}} = -\frac{1}{4\pi}\mathbb{C}^T\mathbb{M}_2\mathbb{C}\cdot\boldsymbol{a} \\[4pt]
H_Y : \ & \dot{\boldsymbol{a}} = 4\pi c^2\mathbb{M}_1^{-1}\cdot\boldsymbol{y} \\[6pt]
H_{\text{Kinetic}}^{\alpha} : \ &
\begin{cases}
\dot{X}_\ell^\alpha = \dfrac{1}{m_\ell}\left(P_{\ell\alpha} - \dfrac{q_\ell}{c}A(X_\ell)_\alpha\right) \\[8pt]
\dot{P}_{\ell\mu} = \dfrac{q_\ell}{c}\dot{X}_\ell^\alpha\partial_{X_\ell^\mu}A(X_\ell)_\alpha \\[8pt]
\dot{\boldsymbol{y}} = \sum\limits_{\ell=1}^{L}\dfrac{q_\ell}{c}\dot{X}_\ell^\alpha\boldsymbol{\Lambda}^1(X_\ell)_\alpha.
\end{cases}
\end{aligned}
\right\}
\tag{5.4}
$$

To clarify the notation in (5.4), we emphasize that, in the $H_{\text{Kinetic}}^{\alpha}$ subsystem, $\dot{X}_\ell^\mu = 0$ for $\mu \neq \alpha$. (Here, α is regarded as fixed while μ ranges over all $\{x, y, z\}$ indices.) Thus, the equations of motion for $X_\ell^{\mu\neq\alpha}$ are omitted above.

Furthermore, it follows from a simple calculation that $\ddot{X}_\ell^\alpha = 0$ in $H_{\text{Kinetic}}^{\alpha}$ so that $\dot{X}_\ell^\alpha$ is constant during the evolution of each subsystem. As a result, all subsystems above are exactly integrable. Equation (5.4) therefore defines a GCSM.

More concretely, an evolution over the timestep $[t, t + \Delta]$ in each subsystem is fully specified by

$$
\left.
\begin{aligned}
H_A : \ & \boldsymbol{y}(t + \Delta) = \boldsymbol{y}(t) - \frac{\Delta}{4\pi}\mathbb{C}^T\mathbb{M}_2\mathbb{C}\cdot\boldsymbol{a}(t) \\[4pt]
H_Y : \ & \boldsymbol{a}(t + \Delta) = \boldsymbol{a}(t) + \Delta 4\pi c^2\mathbb{M}_1^{-1}\cdot\boldsymbol{y}(t) \\[6pt]
H_{\text{Kinetic}}^{\alpha} : \ &
\begin{cases}
X_\ell^\alpha(t + \delta) = X_\ell^\alpha(t) + \dfrac{\delta}{m_\ell}\left(P_{\ell\alpha}(t) - \dfrac{q_\ell}{c}\boldsymbol{a}(t)\cdot\boldsymbol{\Lambda}^1(X_\ell(t))_\alpha\right) \\[8pt]
P_{\ell\mu}(t + \Delta) = P_{\ell\mu}(t) + \dfrac{q_\ell}{c}\dot{X}_\ell^\alpha(t)\boldsymbol{a}(t)\cdot\int\limits_{t}^{t+\Delta}\mathrm{d}t'\partial_{X_\ell^\mu(t')}\boldsymbol{\Lambda}^1(X_\ell(t'))_\alpha \\[8pt]
\boldsymbol{y}(t + \Delta) = \boldsymbol{y}(t) + \sum\limits_{\ell=1}^{L}\dfrac{q_\ell}{c}\dot{X}_\ell^\alpha(t)\int\limits_{t}^{t+\Delta}\mathrm{d}t'\boldsymbol{\Lambda}^1(X_\ell(t'))_\alpha.
\end{cases}
\end{aligned}
\right\}
\tag{5.5}
$$

In (5.5), t is a fixed initial time and $\delta \in [0, \Delta]$ parametrizes the particle trajectory $X_\ell(t) \to X_\ell(t + \Delta)$ during one timestep of the $H_{\text{Kinetic}}^{\alpha}$ subsystem, which forms a straight line segment in the $\hat{\alpha}$ direction. Since $\boldsymbol{\Lambda}^1$ is comprised of piecewise polynomial differential 1-forms, $\boldsymbol{\Lambda}^1$ and its derivatives are integrable in closed form along the straight path $X_\ell(t + \delta)$. Thus, (5.5) defines a symplectic algorithm – specifically a GCSM – that can be computed exactly.

6. Numerical examples

We now demonstrate the efficacy of this algorithm numerically. In §6.1, we first consider a one-dimensional simulation of Landau damping electrons, choosing simulation parameters similar to those of Xiao *et al.* (2015), against a fixed, homogeneous, positive background charge. Then, in §6.2, we reexpress the 1X2V simulation approach pursued in Crouseilles *et al.* (2015) and Kraus *et al.* (2017) in canonical coordinates, thereby
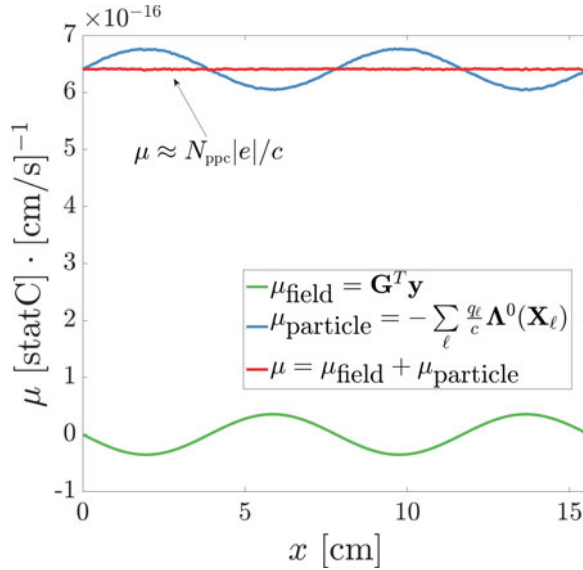
FIGURE 2. The terms of (4.21) are plotted over the simulation domain at time $t = 0$, characterizing initial conditions by the momentum map $\mu = \mu_{\text{field}} + \mu_{\text{particle}}$.

deriving the restriction of our algorithm to 1X2P phase space – comprised of one spatial dimension and two dimensions of canonical momentum. Finally, in § 6.3, we simulate the electromagnetic Weibel instability in this restricted phase space.

6.1. *Landau damping*

Using Whitney form finite elements, a 650-cell domain $\mathcal{T}_h$ with periodic boundaries is constructed. Each cell is assigned width $w_x = 2.4 \times 10^{-2}$ cm, and 26×10^6 electrons are simulated (40 000 per cell, when unperturbed). With electron temperature at $T_e = 5$ keV, the set-up has Debye length $\lambda_D = 1.0$ cm and plasma frequency $\omega_p = 3.0 \times 10^9$ rad s^{-1}, roughly mirroring physical parameters of Xiao *et al.* (2015).

We assume the electric field to have initial perturbation at $t = 0$

$$Y = -\frac{E}{4\pi c} = -\frac{E_0 \cos(kx)}{4\pi c}\hat{x}, \tag{6.1}$$

where $E_0 = 1.2$ statV cm^{-1} and $k\lambda_D = 0.8$. To construct this perturbation, we first project the continuous 1-form field Y_{cont} onto its Whitney form approximation, i.e. $Y_{\text{cont}} \xrightarrow{\pi_h} Y = y \cdot \mathbb{M}_1^{-1} \cdot \Lambda^1$. In particular, we solve for y in (4.3) such that the integrals of Y_{cont} and Y agree on edges of the discretized domain. This procedure yields a sinusoidal $\mu_{\text{field}} = \mathbb{G}^T y$ as depicted in figure 2.

From the particle side, electron momenta are initialized in phase space by randomly selecting their velocities $\dot{X}_\ell$ from a Maxwellian distribution of temperature $T_e = 5$ keV. Taking $A = 0$ at $t = 0$, initial canonical momenta are therefore given by $P_\ell = m_\ell \dot{X}_\ell$. Electron positions are then initialized to be consistent with Gauss' law. More precisely, we demand that particle positions, in combination with the electric field perturbation, ensure the constancy of the total momentum map μ. Following (4.23), a non-zero constant momentum map can be understood as a fixed, homogeneous, ion background charge, $\mu \sim \rho_{\text{ext}}/c$. Indeed, in a Landau damping simulation that takes only electrons

to be dynamical, such a constant background charge constitutes the desired Gauss' law remainder.

We therefore optimize electron positions $\{X_\ell\}$ to ensure $\mu_{\text{particle}} = \sum_\ell (|e|/c) \boldsymbol{\Lambda}^0(X_\ell)$ closely satisfies

$$\mu = \mu_{\text{field}} + \mu_{\text{particle}} \approx N_{\text{ppc}} |e| /c, \qquad (6.2)$$

where $\mu_{\text{field}} = \mathbb{G}^T \boldsymbol{y}$ and $N_{\text{ppc}} = 40\,000$ denotes the number of particles per cell. In this way, the positive background charge, characterized by μ, is homogeneous across the simulation domain and enforces quasineutrality with the dynamical electrons.

This optimization of μ_{particle} is carried out in two stages. First, electrons are randomly selected via rejection sampling (von Neumann 1951) from the distribution

$$n_e(x) = n_0 \left[1 + \frac{k E_0 \sin(kx)}{4\pi |e| n_0} \right], \qquad (6.3)$$

which satisfies $\nabla \cdot \boldsymbol{E} = 4\pi |e| (n_0 - n_e)$. The electron positions $\{X_\ell\}$ are then further optimized using Nesterov accelerated gradient descent (Nesterov 1983) to minimize the objective function

$$\arg \min_{\{X_\ell\}} \left| \mu - \frac{N_{\text{ppc}} |e|}{c} \right|^2. \qquad (6.4)$$

The resulting momentum map, plotted in red in figure 2, thus defines a background charge that is homogeneous to a high degree of accuracy.

Note that an alternative initialization, undertaken for example by Kraus *et al.* (2017), reverses the above procedure by randomly generating electron positions first and then solving for $\boldsymbol{y}$ to satisfy Gauss' law. This alternative is more straightforward computationally than the procedure described above, but it may afford less precision in the specification of the initial electric field perturbation, whenever such precision is desirable.

With initialized fields and electrons, the simulation is then evolved using a first-order Lie–Trotter splitting (Trotter 1959) derived from (5.5), in particular,

$$\boldsymbol{u}(t + \Delta) = \exp(\Delta H^x_{\text{Kinetic}}) \exp(\Delta H_Y) \exp(\Delta H_A) \boldsymbol{u}(t), \qquad (6.5)$$

where $\boldsymbol{u}(t)$ denotes the simulation state at time t – i.e. $\boldsymbol{u} = m_d \in M_d$, a point in phase space as defined in (4.11).

In figure 3, we first examine the evolution of the momentum map throughout the simulation domain. We note that, while μ_{particle} (multicolour) exhibits an oscillation and decay consistent with Landau damping, μ (grey) remains constant over time, consistent with the conservation of the momentum map.

To compare this simulation with theory, the evolution of the (normalized) electric field is plotted in figure 4 (which may be compared with figure 2 of Xiao *et al.* 2015). The results agree with a theoretical expectation of (i) electrostatic Langmuir wave oscillation at a frequency $\omega_p = 3.0 \times 10^9$ rad s^{-1}, and (ii) Landau damping at a decay rate $\omega_i = \omega_p/\kappa^3 \sqrt{(\pi/8)} \exp(-(1 + 3\kappa^2)/2\kappa^2) = 3.9 \times 10^8$ rad s^{-1}, where $\kappa = k\lambda_D$. Furthermore, as is characteristic of a symplectic algorithm, the error in the total energy, measured by H_{VM} of (4.12), is well bounded throughout the simulation. This error is plotted in figure 5.

Having demonstrated the canonical finite element formalism's efficacy in simulating an electrostatic problem, we next consider the electromagnetic simulation of the Weibel instability. Before that, however, we introduce the 'canonical 1X2P phase space' in which we will conduct our simulation.
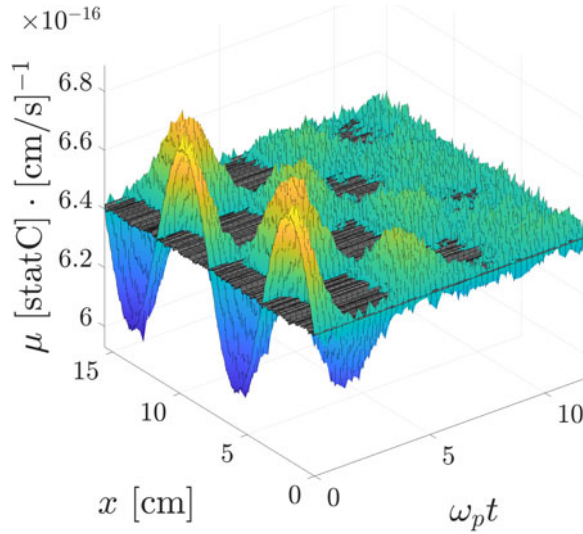
FIGURE 3. With their initial conditions as depicted in figure 2, the total momentum map μ (grey) is compared with μ_{particle} (multicolour) as the two functions evolve over time. Whereas μ_{particle} exhibits a decaying sinusoid consistent with Landau damping, μ remains constant to machine precision. The momentum map μ constitutes a physical representation of the fixed positive background charge implicit in the simulation.
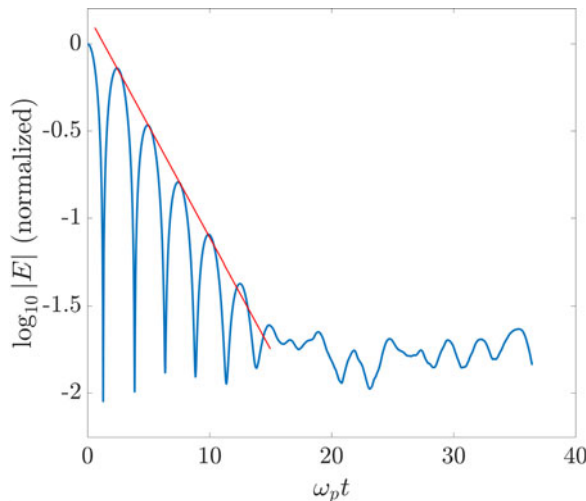

FIGURE 4. The evolution of an electrostatic wave over time is simulated with a first-order Lie–Trotter splitting (Trotter 1959) of (5.5). The blue time series denotes the (normalized) log modulus of the electric field $E = -4\pi c Y$, where $|E|$ is computed over the simulation domain by the $L^2 \Lambda^1$ norm. The theoretical Landau damping rate of the wave in a Maxwellian plasma is depicted as a red line, decaying at a rate of $\omega_i = \omega_p/\kappa^3 \sqrt{(\pi/8)} \exp(-(1 + 3\kappa^2)/2\kappa^2)$ for $\kappa = k\lambda_D$.
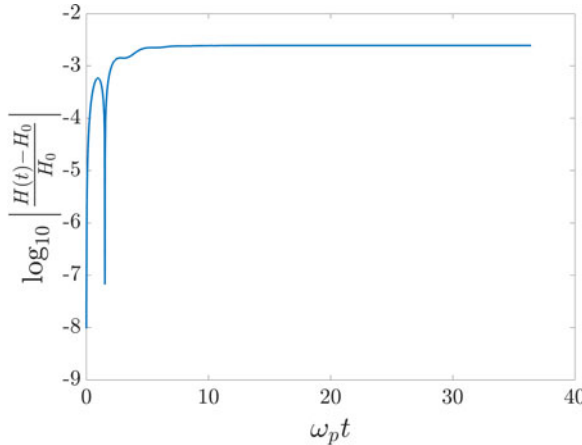
FIGURE 5. The log error in the total energy of a first-order Lie–Trotter splitting (Trotter 1959) Landau damping simulation.

6.2. *Canonical 1X2P phase space*

Let us consider the restriction of phase space to one spatial dimension and two dimensions of canonical momentum. Despite its computational efficiency, the 1X2P setting is capable of simulating a number of non-trivial electromagnetic problems. Our development here of 1X2P phase space essentially adapts for canonical coordinates the techniques of Crouseilles *et al.* (2015) and Kraus *et al.* (2017).

To characterize 1X2P, we must reflect the lack of y dependence in the finite element expansions of our fields. In this setting, we therefore define A and Y by analogy with (4.3) as

$$\left.\begin{array}{c} A = a_x \cdot \Lambda^1(x) + a_y \cdot \Lambda^0(x) \\[4pt] Y = y_x \cdot \mathbb{M}_1^{-1} \cdot \Lambda^1(x) + y_y \cdot \mathbb{M}_0^{-1} \cdot \Lambda^0(x). \end{array}\right\} \tag{6.6}$$

Here, a_x denotes a vector of coefficients that pair only with the finite element 1-form basis $\Lambda^1(x)$ – a basis in 1X2P which has only x-components and whose spatial dependence is only one-dimensional. We further note that a_y is defined as the coefficients of a 0-form. Since there is no way to associate 1-forms with $\hat{y}$-directed edges in the 1X2P setting, 0-forms are the most natural representation of the y components of A. This becomes especially clear when examining finite elements restricted to have spatial x-dependence. The expansion of Y in (6.6) follows similarly, with appropriate mass matrices computed by integrals over the one-dimensional domain.

Turning now to the characterization of particle phase space, we retain two components of the canonical momentum, $P_{\ell x}$ and $P_{\ell y}$. Only one component of spatial dependence is retained, which we shall denote X_ℓ.

The appropriate Hamiltonian is then computed by restricting (4.12) as follows:

$$H_{1X2P} = \frac{1}{8\pi} \left((4\pi c)^2 \left[y_x \cdot \mathbb{M}_1^{-1} \cdot y_x + y_y \cdot \mathbb{M}_0^{-1} \cdot y_y \right] + a_y \cdot \mathbb{G}^T \mathbb{M}_1 \mathbb{G} \cdot a_y \right)$$

$$+ \sum_{\ell=1}^{L} \frac{1}{2m_\ell} \left(\left| P_{\ell x} - \frac{q_\ell}{c} a_x \cdot \Lambda^1(X_\ell) \right|^2 + \left| P_{\ell y} - \frac{q_\ell}{c} a_y \cdot \Lambda^0(X_\ell) \right|^2 \right). \tag{6.7}$$

We note that the term $a_x \cdot \mathbb{C}^T \mathbb{M}_2 \mathbb{C} \cdot a_x$ is absent; while it would ordinarily arise from the magnetic energy $|dA|^2$, d annihilates 1-forms in the 1X2P setting. Indeed, the magnetic field in the 1X2P formalism is given simply by $B = dA = a_y \cdot dA^0 = \mathbb{G}a_y \cdot A^1$.

The Poisson bracket of the restricted phase space follows by simply omitting the inapplicable terms of (4.10). In particular

$$\{F, G\}_{\text{1X2P}} = \left(\frac{\partial F}{\partial a_x} \cdot \frac{\partial G}{\partial y_x} + \frac{\partial F}{\partial a_y} \cdot \frac{\partial G}{\partial y_y} + \sum_{\ell=1}^{L} \frac{\partial F}{\partial X_\ell} \frac{\partial G}{\partial P_{\ell x}} \right) - (F \leftrightarrow G). \quad (6.8)$$

We observe that, despite its simplicity, the 1X2P phase space retains the gauge structure of the original problem. In particular we note its gauge symmetry

$$\Phi_{\exp(s)} \begin{pmatrix} a_x \\ P_{\ell x} \end{pmatrix} = \begin{pmatrix} a_x + \mathbb{G}s_x \\ P_{\ell x} + \dfrac{q_\ell}{c} \mathbb{G}s_x \cdot A^1(X_\ell)_x \end{pmatrix}, \quad (6.9)$$

and the resulting momentum map

$$\mu_{\text{1X2P}} = \mathbb{G}^T y_x - \sum_{\ell=1}^{L} \frac{q_\ell}{c} A^0(X_\ell). \quad (6.10)$$

Finally, we derive the equations of motion in the 1X2P setting, which are straightforward reexpressions of their full phase space counterparts in (5.1)

$$\left.\begin{aligned}
\dot{X}_\ell &= \{X_\ell, H_{\text{1X2P}}\} = \frac{1}{m_\ell} \left(P_{\ell x} - \frac{q_\ell}{c} a_x \cdot A^1(X_\ell) \right) \\
\dot{P}_{\ell x} &= \{P_{\ell x}, H_{\text{1X2P}}\} = \frac{q_\ell}{c} \left[\dot{X}_\ell a_x \cdot \left(\partial_{X_\ell} A^1(X_\ell) \right) + \dot{Y}_\ell a_y \cdot \left(\partial_{X_\ell} A^0(X_\ell) \right) \right] \\
\dot{a}_x &= \{a_x, H_{\text{1X2P}}\} = 4\pi c^2 \mathbb{M}_1^{-1} \cdot y_x \\
\dot{a}_y &= \{a_y, H_{\text{1X2P}}\} = 4\pi c^2 \mathbb{M}_0^{-1} \cdot y_y \\
\dot{y}_x &= \{y_x, H_{\text{1X2P}}\} = \sum_{\ell=1}^{L} \frac{q_\ell}{c} \dot{X}_\ell A^1(X_\ell) \\
\dot{y}_y &= \{y_y, H_{\text{1X2P}}\} = \sum_{\ell=1}^{L} \frac{q_\ell}{c} \dot{Y}_\ell A^0(X_\ell) - \frac{1}{4\pi} \mathbb{G}^T \mathbb{M}_1 \mathbb{G} \cdot a_y.
\end{aligned}\right\} \quad (6.11)$$

Here, with an abuse of notation that ignores the non-existence of Y_ℓ, we define

$$\dot{Y}_\ell = \frac{1}{m_\ell} \left(P_{\ell y} - a_y \cdot A^0(X_\ell) \right). \quad (6.12)$$

We observe that $P_{\ell y}$ is conserved in (6.11), which can be viewed as a consequence of the independence from Y_ℓ of the 1X2P formulation.

We further note that a gauge-compatible splitting of H_{1X2P} is readily defined by the following four sub-Hamiltonians, in agreement with (5.3)

$$
\left.
\begin{aligned}
H_{1X2P} &= H_A + H_Y + H_{\text{Kinetic}}^x + H_{\text{Kinetic}}^y \\
\text{where} \quad H_A &= \frac{1}{8\pi} \boldsymbol{a}_y \cdot \mathbb{G}^T \mathbb{M}_1 \mathbb{G} \cdot \boldsymbol{a}_y \\
H_Y &= \frac{1}{8\pi} \left((4\pi c)^2 \left[\boldsymbol{y}_x \cdot \mathbb{M}_1^{-1} \cdot \boldsymbol{y}_x + \boldsymbol{y}_y \cdot \mathbb{M}_0^{-1} \cdot \boldsymbol{y}_y \right] \right) \\
H_{\text{Kinetic}}^x &= \sum_{\ell=1}^{L} \frac{1}{2m_\ell} \left| P_{\ell x} - \frac{q_\ell}{c} \boldsymbol{a}_x \cdot \boldsymbol{\Lambda}^1(X_\ell) \right|^2 \\
H_{\text{Kinetic}}^y &= \sum_{\ell=1}^{L} \frac{1}{2m_\ell} \left| P_{\ell y} - \frac{q_\ell}{c} \boldsymbol{a}_y \cdot \boldsymbol{\Lambda}^0(X_\ell) \right|^2 .
\end{aligned}
\right\}
\tag{6.13}
$$

Using the Poisson bracket $\{\cdot, \cdot\}_{1X2P}$ of (6.8), we thereby derive the following subsystem equations of motion:

$$
H_A : \left\{ \dot{\boldsymbol{y}}_y = -\frac{1}{4\pi} \mathbb{G}^T \mathbb{M}_1 \mathbb{G} \cdot \boldsymbol{a}_y \right. \qquad\qquad H_Y : \left\{ \begin{aligned} \dot{\boldsymbol{a}}_x &= 4\pi c^2 \mathbb{M}_1^{-1} \cdot \boldsymbol{y}_x \\ \dot{\boldsymbol{a}}_y &= 4\pi c^2 \mathbb{M}_0^{-1} \cdot \boldsymbol{y}_y \end{aligned} \right.
$$

$$
H_{\text{Kinetic}}^x : \begin{cases} \dot{X}_\ell = \dfrac{1}{m_\ell} \left(P_{\ell x} - \dfrac{q_\ell}{c} \boldsymbol{a}_x \cdot \boldsymbol{\Lambda}^1(X_\ell) \right) \\ \dot{P}_{\ell x} = \dfrac{q_\ell}{c} \dot{X}_\ell \boldsymbol{a}_x \cdot \left(\partial_{X_\ell} \boldsymbol{\Lambda}^1(X_\ell) \right) \\ \dot{\boldsymbol{y}}_x = \sum_{\ell=1}^{L} \dfrac{q_\ell}{c} \dot{X}_\ell \boldsymbol{\Lambda}^1(X_\ell) \end{cases} \qquad H_{\text{Kinetic}}^y : \begin{cases} \dot{P}_{\ell x} = \dfrac{q_\ell}{c} \dot{Y}_\ell \boldsymbol{a}_y \cdot \left(\partial_{X_\ell} \boldsymbol{\Lambda}^0(X_\ell) \right) \\ \dot{\boldsymbol{y}}_y = \sum_{\ell=1}^{L} \dfrac{q_\ell}{c} \dot{Y}_\ell \boldsymbol{\Lambda}^0(X_\ell). \end{cases}
$$

$$
\tag{6.14}
$$

Since these equations of motion are – as (5.5) – exactly solvable, and since the sub-Hamiltonians of (6.13) preserve the gauge symmetry of (6.9), it is clear that (6.14) defines a GCSM that exactly preserves μ_{1X2P}.

6.3. *Weibel instability*

We now apply the 1X2P formulation defined above to the simulation of the Weibel instability. We initialize the simulation in close agreement with the parametrization of the Weibel instability simulations of Crouseilles *et al.* (2015) and Kraus *et al.* (2017). Specifically, in a periodic domain of 64 cells we simulate $N_e = 100\,032$ electrons. Continuing to work in Gaussian units, we take perturbation wavenumber $k = 1.25(\omega_p/c)$ and simulation domain length $L = 2\pi/k$. We seed a magnetic perturbation by defining the vector potential to be

$$
A = \frac{B_0}{k} \sin(kx)\hat{y}, \tag{6.15}
$$

where $B_0 = -5.7\,\text{mG}$. We sample initial electron velocities from the anisotropic distribution

$$
f_e(x, v_x, v_y) = \frac{1}{2\pi\sigma_x\sigma_y} \exp\left(-\left[\frac{v_x^2}{2\sigma_x^2} + \frac{v_y^2}{2\sigma_y^2} \right] \right), \tag{6.16}
$$

where $\sigma_x = 0.02c/\sqrt{2}$ and $\sigma_y = \sqrt{12}\sigma_x$. To initialize the initial electron distribution to be independent of x (i.e. spatially uniform) as above, we evenly space electrons throughout
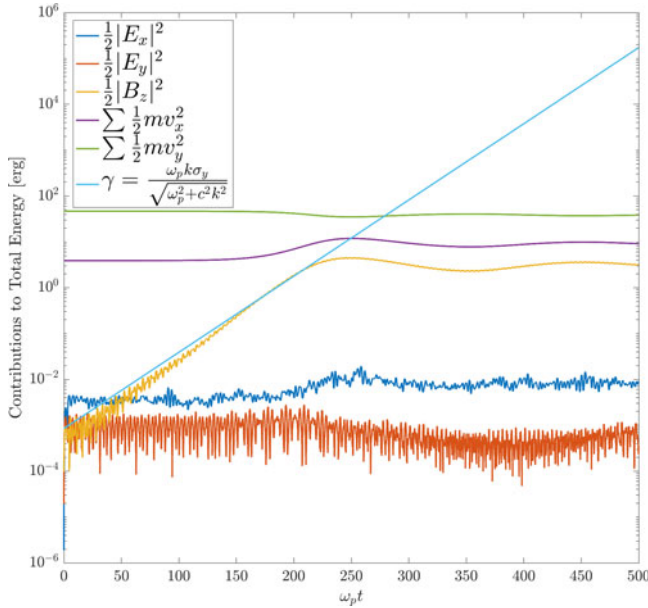
FIGURE 6. The growth rate of the magnetic field energy closely approximates the analytic model of the Weibel instability. As the magnetic field ramps up, the anisotropy of the electron velocity is reduced. This plot may be compared with figure 1 of Kraus *et al.* (2017).

the simulation domain at separation of L/N_e. Y is correspondingly initialized to zero. A and Y are again modelled using Whitney (0- and 1-) forms.

Finally, simulating the Weibel instability with a Lie–Trotter splitting of stepsize $1/40\omega_p$ yields the evolution plotted in figure 6. The magnetic field growth rate is in strong agreement with the analytic prediction (Weibel 1959),

$$\gamma = \frac{\omega_p k \sigma_y}{\sqrt{\omega_p^2 + c^2 k^2}}. \tag{6.17}$$

Lastly, the total energy is also well bounded over the lifetime of the Weibel instability simulation, as depicted in figure 7.

7. Conclusion

We have derived a canonical Poisson structure in (4.10) for the Vlasov–Maxwell system and constructed its Hamiltonian in (4.12) in the formalism of FEEC. Its gauge symmetry was studied to systematically derive the corresponding charge-conserving momentum map of (4.21). The resulting PIC algorithm of (5.5) was demonstrated to be a GCSM that preserves the momentum map to machine precision over the full simulation domain.

We have seen in (4.23) how the momentum map may be regarded as an external fixed charge in a PIC simulation. Using this interpretation, we optimized initial conditions for a Landau damping simulation that modelled a homogeneous positive fixed background, as depicted in figure 2. We explicitly demonstrated the preservation of this momentum map, as seen in figure 3.

The initialization procedure we described may be useful in future structure-preserving PIC simulations that require the precise initial specification of electric fields and
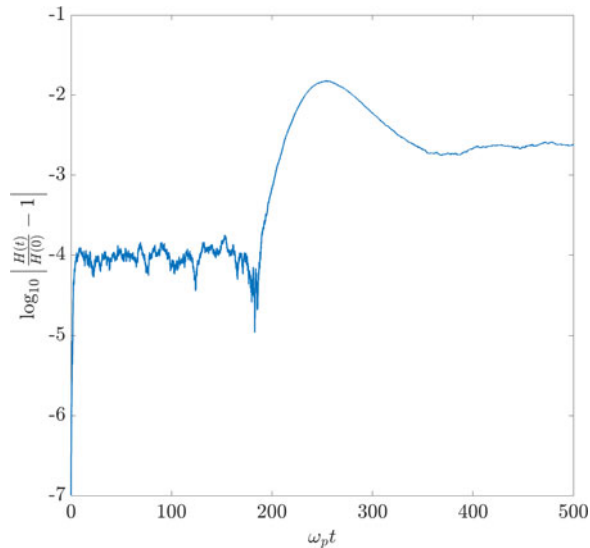
FIGURE 7. The log error in the total energy of a first-order Lie–Trotter splitting (Trotter 1959) Weibel instability simulation (Weibel 1959).

background charge. Such a technique might be advantageous, for example, in the simulation of plasma interactions with charged plasma-facing components.

We further explored the efficacy of our gauge-compatible splitting algorithm by examining its restriction to 1X2P phase space, in which setting we simulated the Weibel instability. We demonstrated that the gauge structure of the full phase space has a counterpart in this sparser setting, and we accurately modelled the analytic growth rate of the Weibel instability in our simulation.

The flexibility of FEEC makes the algorithms defined in this paper significantly generalizable as well. For example, the PIC algorithm of this paper may be adapted to simulations on an unstructured mesh, including perhaps those defined in curvilinear coordinates.

However, it is worth noting an important drawback to the use of higher-order finite element spaces in the foregoing algorithms, namely, that their inverse mass matrices (e.g. $\mathbb{M}_1^{-1}$ in (5.4)) are not, in general, sparse. Dense inverse mass matrices necessitate global communication in every timestep of a simulation, significantly reducing the benefit of parallelization. Overcoming such a limitation would facilitate scalable, higher-order and higher-dimensional simulations – an effort that will be worthy of future study.

Acknowledgements

Funding

opinions expressed in this paper are the authors' and do not necessarily reflect the policies and views of DOE, ORAU, or ORISE.

Declaration of interests

The authors report no conflict of interest.

Author contributions

The authors contributed equally to theoretical development. A.S.G. performed the derivations and simulations.

REFERENCES

ARNOLD, D.N. & AWANOU, G. 2013 Finite element differential forms on cubical meshes. *Maths Comput.* **83** (288), 1551–1570.

ARNOLD, D.N., BOFFI, D. & BONIZZONI, F. 2015 Finite element differential forms on curvilinear cubic meshes and their approximation properties. *Numer. Math.* **129** (1), 1–20.

ARNOLD, D.N., FALK, R.S. & WINTHER, R. 2006 Finite element exterior calculus, homological techniques, and applications. *Acta Numerica* **15**, 1–155.

ARNOLD, D.N., FALK, R.S. & WINTHER, R. 2010 Finite element exterior calculus: from Hodge theory to numerical stability. *Bull. Am. Math. Soc.* **47** (2), 281–354.

BURBY, J.W. 2017 Finite-dimensional collisionless kinetic theory. *Phys. Plasmas* **24** (3), 032101.

CROUSEILLES, N., EINKEMMER, L. & FAOU, E. 2015 Hamiltonian splitting for the Vlasov–Maxwell equations. *J. Comput. Phys.* **283**, 224–240.

ESIRKEPOV, T. 2001 Exact charge conservation scheme for particle-in-cell simulation with an arbitrary form-factor. *Comput. Phys. Commun.* **135** (2), 144–153.

EVSTATIEV, E. & SHADWICK, B. 2013 Variational formulation of particle algorithms for kinetic plasma simulations. *J. Comput. Phys.* **245**, 376–398.

GLASSER, A.S. & QIN, H. 2020 The geometric theory of charge conservation in particle-in-cell simulations. *J. Plasma Phys.* **86** (3), 835860303.

HE, Y., QIN, H., SUN, Y., XIAO, J., ZHANG, R. & LIU, J. 2015 Hamiltonian time integrators for Vlasov–Maxwell equations. *Phys. Plasmas* **22** (12), 124503.

HE, Y., SUN, Y., QIN, H. & LIU, J. 2016 Hamiltonian particle-in-cell methods for Vlasov–Maxwell equations. *Phys. Plasmas* **23** (9), 092108.

HIRVIJOKI, E., KORMANN, K. & ZONTA, F. 2020 Subcycling of particle orbits in variational, geometric electromagnetic particle-in-cell methods. *Phys. Plasmas* **27**, 092506.

HOLDERIED, F., POSSANNER, S. & WANG, X. 2021 MHD-kinetic hybrid code based on structure-preserving finite elements with particles-in-cell. *J. Comput. Phys.* **433**, 110143.

KORMANN, K. & SONNENDRÜCKER, E. 2021 Energy-conserving time propagation for a structure-preserving particle-in-cell Vlasov–Maxwell solver. *J. Comput. Phys.* **425**, 109890.

KRAUS, M. & HIRVIJOKI, E. 2017 Metriplectic integrators for the Landau collision operator. *Phys. Plasmas* **24** (10), 102311.

KRAUS, M., KORMANN, K., MORRISON, P.J. & SONNENDRÜCKER, E. 2017 GEMPIC: geometric electromagnetic particle-in-cell methods. *J. Plasma Phys.* **83** (4), 905830401.

MARSDEN, J. & RATIU, T. 1999 *Introduction to Mechanics and Symmetry*, 2nd edn. Texts in Applied Mathematics, vol. 17. Springer.

MARSDEN, J. & WEINSTEIN, A. 1974 Reduction of symplectic manifolds with symmetry. *Rep. Math. Phys.* **5** (1), 121–130.

MARSDEN, J.E. & RATIU, T. 1986 Reduction of Poisson manifolds. *Lett. Math. Phys.* **11** (2), 161–169.

MARSDEN, J.E. & WEINSTEIN, A. 1982 The Hamiltonian structure of the Maxwell–Vlasov equations. *Physica* D **4** (3), 394.

MOON, H., TEIXEIRA, F.L. & OMELCHENKO, Y.A. 2015 Exact charge-conserving scatter–gather algorithm for particle-in-cell simulations on unstructured grids: a geometric perspective. *Comput. Phys. Commun.* **194**, 43–53.

MORRISON, P.J. 2017 Structure and structure-preserving algorithms for plasma physics. *Phys. Plasmas* **24** (5), 055502.

NESTEROV, Y.E. 1983 A method of solving a convex programming problem with convergence rate $O(1/k^2)$. *Dokl. Akad. Nauk SSSR* **269** (3), 543.

VON NEUMANN, J. 1951 Various techniques used in connection with random digits. In *Monte Carlo Method*, National Bureau of Standards Applied Mathematics Series, vol. 12, pp. 36–38. US Government Printing Office.

O'CONNOR, S., CRAWFORD, Z.D., RAMACHANDRAN, O.H., LUGINSLAND, J. & SHANKER, B. 2021 Time integrator agnostic charge conserving finite element PIC. *Phys. Plasmas* **28** (9), 092111.

PERSE, B., KORMANN, K. & SONNENDRÜCKER, E. 2021 Geometric particle-in-cell simulations of the Vlasov–Maxwell system in curvilinear coordinates. *SIAM J. Sci. Comput.* **43** (1), B194–B218.

PINTO, M.C., KORMANN, K. & SONNENDRÜCKER, E. 2022 Variational framework for structure-preserving electromagnetic particle-in-cell methods. *J. Sci. Comput.* **91** (46), 1–39.

QIN, H., HE, Y., ZHANG, R., LIU, J., XIAO, J. & WANG, Y. 2015 Comment on "Hamiltonian splitting for the Vlasov–Maxwell equations". *J. Comput. Phys.* **297**, 721–723.

QIN, H., LIU, J., XIAO, J., ZHANG, R., HE, Y., WANG, Y., SUN, Y., BURBY, J.W., ELLISON, L. & ZHOU, Y. 2016 Canonical symplectic particle-in-cell method for long-term large-scale simulations of the Vlasov–Maxwell equations. *Nucl. Fusion* **56** (1), 014001.

DA SILVA, A.C. 2001 *Lectures on Symplectic Geometry*. Lecture Notes in Mathematics, vol. 1764. Springer.

SOURIAU, J.-M. 1970 *Structure des systèmes dynamiques*. Dunod.

SQUIRE, J., QIN, H. & TANG, W.M. 2012 Geometric integration of the Vlasov–Maxwell system with a variational particle-in-cell scheme. *Phys. Plasmas* **19** (8), 084501.

TROTTER, H.F. 1959 On the product of semi-groups of operators. *Proc. Am. Math. Soc.* **10** (4), 545–551.

VILLASENOR, J. & BUNEMAN, O. 1992 Rigorous charge conservation for local electromagnetic field solvers. *Comput. Phys. Commun.* **69** (2–3), 306–316.

WANG, Z., QIN, H., STURDEVANT, B. & CHANG, C. 2021 Geometric electrostatic particle-in-cell algorithm on unstructured meshes. *J. Plasma Phys.* **87** (4), 905870406.

WEIBEL, E.S. 1959 Spontaneously growing transverse waves in a plasma due to an anisotropic velocity distribution. *Phys. Rev. Lett.* **2** (3), 83–84.

WHITNEY, H. 1957 *Geometric Integration Theory*. Princeton University Press.

XIAO, J., LIU, J., QIN, H. & YU, Z. 2013 A variational multi-symplectic particle-in-cell algorithm with smoothing functions for the Vlasov–Maxwell system. *Phys. Plasmas* **20** (10), 102517.

XIAO, J. & QIN, H. 2019 Field theory and a structure-preserving geometric particle-in-cell algorithm for drift wave instability and turbulence. *Nucl. Fusion* **59** (10), 106044.

XIAO, J. & QIN, H. 2021 Explicit structure-preserving geometric particle-in-cell algorithm in curvilinear orthogonal coordinate systems and its applications to whole-device 6D kinetic simulations of tokamak physics. *Plasma Sci. Technol.* **23** (5), 055102.

XIAO, J., QIN, H. & LIU, J. 2018 Structure-preserving geometric particle-in-cell methods for Vlasov–Maxwell systems. *Plasma Sci. Technol.* **20** (11), 110501.

XIAO, J., QIN, H., LIU, J., HE, Y., ZHANG, R. & SUN, Y. 2015 Explicit high-order non-canonical symplectic particle-in-cell algorithms for Vlasov–Maxwell systems. *Phys. Plasmas* **22** (11), 112504.